An index of anomalous convective instability to detect tornadic and hail storms

Weihong Qian[1]*, Jeremy Cheuk-Hin Leung[1], Weimeng Luo[1], Jun Du[2], and Jidong Gao[3]

[1] *Department of Atmospheric and Oceanic Sciences, School of Physics, Peking University, Beijing 100871*

[2] *NOAA/NCEP/Environmental Modeling Center, College Park, Maryland, USA*

[3] *NOAA/OAR/National Severe Storms Laboratory, Norman, Oklahoma, USA*

Correspondence to: Weihong Qian, qianwh@pku.edu.cn

Revised and Submitted to *Meteorology and Atmospheric Physics*

(15 Nov, 2017)

Abstract

In this article, the synoptic-scale spatial structures for raising tornadic and hail storms are compared by analyzing the total and anomalous variable fields from the troposphere to the stratosphere. 15 cases of tornado outbreaks and 20 cases of hail storms occurred in the central United States during 1980–2011 were studied. The anomalous temperature-height field shows that a tornadic or hail storm usually occurs at the boundary of anomalous warm and cold air masses horizontally in the troposphere. In one side, an anomalous warm air mass in the mid-low troposphere and an anomalous cold air mass in the stratosphere are vertically separated by a positive center of height anomalies at the upper troposphere. In another side, an opposite vertical pattern shows that an anomalous cold air mass in the mid-low troposphere and an anomalous warm air mass in the stratosphere are separated by a negative center of height anomalies at the upper troposphere. Therefore, two pairs of adjacent anomalous warm/cold centers and one pair of anomalous high/low centers combining together form a major tornadic or hail storm paradigm, which can be physically considered as the storage of anomalous potential energy (APE) to generate severe weather. To quantitatively measure the APE, we define an index of anomalous convective instability (ACI) which is a difference of integrating temperature anomalies based on two vertically opposite anomalous air masses. The APE transformation to anomalous kinetic energy, which reduces horizontal and vertical gradients of temperature anomalies, produces anomalous rising and sinking flows in the lower-layer anomalous warm and cold air mass sides respectively. The intensity of ACI index for tornadic storm cases is 1.5 times larger than that of hail storm cases in average. Thus, this expression of anomalous variables is better than total variables used in the traditional synoptic chart and the ACI index is better than other indices to detect potential tornadic and hail storms in order to understand the environmental conditions

48 affecting severe weather in analytical and model output datasets.

49

50 **1 Introduction**

51 Extreme weather events, such as heat wave, cold surge, heavy rainfall and unusual tropical
52 cyclone frequently hit some places in the world. Locating and forecasting these events are a
53 challenge for meteorologists. In recent years, an approach of anomaly-based analysis has been
54 introduced in studying extreme weather events by Qian et al. (2016a), Chen et al. (2016), Jiang et
55 al. (2016) and Huang et al. (2015) respectively. Particularly, we want to further examine whether
56 the same approach can be used to indicate severe weather such as tornadic and hail storms
57 because both are the most extreme in the world. Qian et al. (2017a) recently studied six historical
58 tornadic storm events in the lower Huaihe River basin of eastern China during 1979–2016 using
59 the approach of anomaly-based analysis. They found that tornadic storms always occur in the
60 warm-wet side from both of anomalous warm and cold air masses separated by the trough axes
61 of negative low-level height anomalies. They further found that the ECMWF model and the
62 NCEP GFS can predict the trough-axis location for leading 42 and 18 hours in advance
63 respectively. Previous studies show that the predicting ability of anomalous variables, such as for
64 height and temperature anomalies, from the ECMWF model can reach 6–7 days in advance in
65 eastern China (Qian et al. 2013; Chen et al. 2016) and 7–8 days in advance in the central United
66 States to the North Atlantic (Bassil 2014; Qian 2017c). It means that the current operational
67 numerical weather prediction models have adequate ability to predict anomalous synoptic
68 precursors indicating weather extremes for leading about a week.

69 The central United States is home to the most frequent violent tornadic storms on Earth
70 (Doswell et al. 2012). In most cases, multiple tornado occurrences can observe within a single

71 synoptic-scale system in the central and southern United States. Although a tornado track
72 warning is usually limited within 10–20 minutes, many studies always adhere to pursuing their
73 goal to find notable synoptic precursors and environmental conditions by using the traditional
74 synoptic charts and dynamical (or thermo-dynamical) diagnostic methods (Agee et al. 1975;
75 Bunkers et al. 2006; Metz and Bosart 2010; Corfidi et al. 2010; Thompson and Edwards 2000).
76 Particularly, Mercer et al. (2012) assessed the differences between tornadic and non-tornadic
77 storms using synoptic-scale pattern composites in the United States. The Glossary of
78 Meteorology (Glickman 2000) describes a tornado outbreak as "multiple tornado occurrences
79 within a single synoptic-scale system". Thus, identifying and expressing synoptic-scale systems
80 that favor tornadic storm is critical if model prediction skill can reach several days in advance.
81 In this study, the synoptic-scale environmental condition for raising tornadic and hail storms
82 are compared by analyzing the total and anomalous variable fields from the troposphere to the
83 stratosphere. The other goal of this study is to construct a new index of anomalous convective
84 instability that is different from traditional severe weather indices and can distinguish tornado
85 outbreaks from hail storms in the central United States. After this introduction, datasets and the
86 anomaly-based approach are described in section 2. The spatial distributions of anomalous
87 variables indicating synoptic-scale systems for tornadic/non-tornadic storm cases are given in
88 sections 3. In section 4, the new index of anomalous convective instability is proposed and
89 compared with other indices. Conclusion and discussion are summarized in section 5.
90

91 **2 Datasets and approach**

92 To identify synoptic-scale systems which may favor the formation of severe weather, four
93 datasets and a case of tornadic storm are used in this article. The first is the CMORPH (CPC

94 MORPHing technique) precipitation dataset that has 3-hourly temporal and 0.25-degree
95 horizontal spatial resolutions, derived from satellite observations (Joyce et al. 2004). The second
96 is the European Centre for Medium-Range Weather Forecasts (ECMWF) Re-Analysis Interim
97 (ERA-Interim) data (Dee et al. 2011) that has a resolution of $0.75° \times 0.75°$ in latitude and
98 longitude at 37 pressure levels, obtained from http://www.ecmwf.int/research/era/do/get/index or
99 http://apps.ecmwf.int/datasets/data/interim_full_daily. The third is the tornado/severe
100 thunderstorm database that records the tornado and non-tornadic severe thunderstorm reports
101 (Schaefer and Edwards 1999; Verbout et al. 2006). The fourth is the convective available
102 potential energy (CAPE) data from the North American Regional Reanalysis (NARR) (Mesinger
103 et al. 2006). The NARR data has an approximate resolution of 0.3 degrees (32 km) in space and
104 a 3-hour interval in time.

105 Using a simple and flexible method, Doswell et al. (2006) has ranked the top-20 tornadic
106 storms and the top-20 days with primarily non-tornadic severe weather (only hail storms) during
107 the period 1970−2003. For the top-20 tornadic storms, the five cases (3 Apr 1974, 27 May 1973,
108 17 Apr 1970, 21 Feb 1971, and 20 Mar 1976) occurred before 1979 are not analyzed in this
109 paper because the ERA-Interim product is available since 1979. We examine the height and
110 temperature anomalies for other 15 cases of tornadic storms after 1979 using the ERA-Interim
111 product and the tornado/severe thunderstorm database. In Table 5 of Doswell et al. (2006), two
112 tornadic storm cases occurred within the same day on 13 Mar 1990 and are considered as one
113 case in this study. Therefore, only 14 cases of tornadic storm, together with an additional special
114 case on 27 to 28 Apr 2011, are analyzed in this paper (Table 1).

115 The tornadic storm during 27–28 Apr 2011 is first studied in the spatial comparison of total
116 and anomalous variable distributions. In April 2011, around 758 tornadoes occurred in America.

During 25–28 Apr 2011, 350 tornadoes occurred from Texas (TX) to eastern Virginia (VA), causing 321 fatalities (Simmons and Sutter 2012). On 27 Apr 2011, the number of tornadoes reached 199, causing 316 deaths (the most casualties in a 24-h period), and more than 2700 injuries. Three distinct episodes of tornadoes over this 24-h period (0500 UTC 27 Apr to 0500 UTC 28 Apr 2011) showed a mesoscale convective system (MCS), a quasi-linear convective system (QLCS), and widespread discrete supercell storms in succession (Knupp et al. 2014). These mesoscale convective systems and supercell storms were directly associated with and raised by a single synoptic-scale system (Qian 2017c).

In our previous studies (Qian 2017c), daily extreme weather events such as heavy rainfall and severe weather storms were seen as results of anomalous synoptic-scale systems related to temporal climatology. The temporal climatology of a certain location and a certain time is considered as a state under the thermodynamic equilibrium of earth-atmosphere system, which is only forced by the solar radiation (solar declination) and surface conditions rather than daily weather disturbances. Thus, an hourly atmospheric total or full field $F_{\{d,y\}}(\lambda,\varphi,p,t)$ such as geopotential height and temperature at diurnal time t (24 hours a day), for a particular time on a calendar date d in a year y at a spatial point of longitude λ and latitude φ, and pressure level p, is decomposed into an hourly climatic field $\bar{F}_d(\lambda,\varphi,p,t)$ and an hourly anomalous field $F'_{\{d,y\}}(\lambda,\varphi,p,t)$ following Qian et al. (2014):

$$F_{\{d,y\}}(\lambda,\varphi,p,t)=\bar{F}_d(\lambda,\varphi,p,t)+F'_{\{d,y\}}(\lambda,\varphi,p,t) \quad (1)$$

The hourly climatic field is estimated by averaging over M years based on the reanalysis data on the calendar date d and at the diurnal time t,

$$\overline{F}_d(\lambda,\varphi,p,t)=\sum_{y=1}^{M}F_{(d,y)}(\lambda,\varphi,p,t)/M \qquad (2)$$

where y runs for M years such as 30 to 100 years. It is assumed that the positive and negative anomalies of meteorological variables at a specific grid point and a given calendar time cancel each other during the M years. The climatic state (or climatology) defined by Eq. (2) contains diurnal cycle since it varies temporally from hour to hour. In previous studies (Qian et al. 2014; Huang et al. 2015), y runs from 1981 to 2010 for M=30 years. To prove the robustness of the resulting climatology, Qian and Huang (2017b) have tested the climatology with and without a super typhoon for 30 years and found the difference to be negligible. Their studies showed that typhoon track forecast using hourly climatic wind on the same calendar day is more accurate than that using a several-day-mean climatic wind.

3 Anomalous synoptic systems for tornadic and non-tornadic cases

Many previous studies (Maddox et al. 1980; Markowski et al. 1998; Rasmussen et al. 2000; Wurman et al. 2007) showed that tornadogeneses can be influenced by the interaction of an ongoing supercell with a preexisting air-mass boundary. As indicated by Schultz et al. (2014), some supercell storms move along or across air-mass boundaries such as warm fronts, stationary fronts, or outflow boundaries produced by other storms. The likelihood of tornado formation may locally increase in these areas because of the enhanced wind shear and moisture near the boundary. In these cases, the temperature gradient along a front is a favorable environment condition for tornadic supercells. For our case, the tornadic outbreak on 27 Apr 2011 was the major component of an extended 4-day disastrous tornado event from 25 Apr to 28 Apr 2011 following a synoptic-scale system moving eastward. On 25 Apr 2011, about 64 tornadoes (only

four with EF-2 or greater in intensity) accompanied with the first rainfall process were spawned between northeast TX, western Tennessee (TN), and Kentucky (KY). On 26 Apr 2011, approximately 50 tornadoes with the second rainfall process occurred from eastern TX to the western parts of TN and KY. After three catastrophic days of the tornadic storm and the third rainfall process on 27 Apr 2011, the residual synoptic-scale system produced 43 additional tornadoes (four with EF-2 and one with EF-3) from Georgia (GA) to New York (NY). For this case, horizontal distributions at 925 hPa and vertical profiles of temperature-height anomalies have been given by Qian (2017c). The comparison between total and climatic fields for the case is additionally given in this section.

Figure 1 compares the horizontal distributions of total height and temperature, climatic height and temperature, and height and temperature anomalies at 925 hPa at four different occasions. The horizontal traditional synoptic chart, climatic synoptic chart and anomalous synoptic chart can be compared in Figs. 1a, 1b and 1c, respectively. At 1200 UTC 27 Apr 2011, tornado tracks and strong rainfall were observed over a relatively broad area of total height and temperature gradients as shown in the traditional synoptic chart (Fig. 1a1), but not within the maximum temperature gradient (or front). Figure 1b shows that the climatic temperature field is mostly parallel to latitude lines and the zonal departures are the results of sea-land contrast. Thus, there is a strong center of climatic temperature varying with diurnal cycle over the southwest United States. After removing the climatic height and temperature (Fig. 1b1) from the total height and temperature, we found that tornado tracks and rainfall occurred near the boundary of anomalous warm and cold air masses as shown on the anomalous synoptic chart (Fig. 1c1). The same feature was also observed at other three occasions. At 0000 UTC 28 Apr 2011, most strong tornadoes with the longest track were also located near the boundary of

183 anomalous warm and cold air masses within the warm side (Fig. 1c3). The trough of height
184 anomalies was basically along the zero line of temperature anomalies, separating an anomalous
185 warm air mass and an anomalous cold air mass. It is clear that the central locations of height and
186 temperature anomalies are different from that of total height and temperature (Fig. 1a vs. Fig.
187 1c). A small negative center of temperature anomalies near the low center (Lt) was influenced by
188 the heavy rainfall (Figs. 1c1 and 1c2).

189 Similarly, Fig. 2 reveals the vertical distributions of total height and temperature, climatic
190 height and temperature, and height and temperature anomalies along different latitudes at the
191 four occasions. The vertical traditional synoptic chart, climatic synoptic chart and anomalous
192 synoptic chart can be compared in Figs. 2a, 2b and 2c, respectively. At 1200 UTC 27 Apr (Fig.
193 2a1), waves in the total height field were weaker than that of total temperature. The diurnal-cycle
194 pattern of climatic temperature is also clearly observed in Fig. 2b with a strong warm center over
195 the southwest United States as compared from Fig. 1b. The anomalous synoptic charts show that
196 rainfall centers and tornadoes were touched down horizontally near the boundary between an
197 anomalous warm mass (a warm air column) and an anomalous cold air mass (a cold air column)
198 and vertically near the low axis of height anomalies in the troposphere (Fig. 2c1). Ascending
199 flow and tornado tracks were located in the anomalous warm air mass side while descending
200 flow was situated in the anomalous cold air mass side. Waves in the total temperature field
201 became stronger from 1800 UTC 27 to 0000 UTC 28 Apr 2011 (Figs. 2a2 and 2a3). In the
202 anomalous synoptic charts (Figs. 2c2 and 2c3), four centers of temperature anomalies indicate
203 two anomalous warm air masses (W2 and W3) and two anomalous cold air masses (C2 and C3),
204 which vertically show a baroclinic pattern (or structure) of height and temperature anomalies. An
205 anomalous high center H3 at the upper troposphere separated the anomalous warm air mass (W3)

below and the anomalous cold air mass (C3) above while an anomalous low center (L2) at the upper troposphere separated the cold air mass (C2) below and the warm air mass (W2) above. Height and temperature anomalies satisfy the hydrostatic balance relationship vertically. It means that the vertical pattern of temperature anomalies can be derived by height anomalies from the troposphere to the stratosphere.

Why were the tornadic storm and heavy rainfall physically associated with the two pairs of adjacent anomalous air masses? In the troposphere below 300 hPa, there were an anomalous warm air mass (W3) in the east side of tornadic storm and an anomalous cold air mass (C2) in the west side. On the stratosphere, however, an anomalous cold air mass (C3) and an anomalous warm air mass (W2) were located in the east and west sides of the tornadic storm respectively. Thermodynamically and vertically, the anomalous warm air mass (W3) below the anomalous cold air mass (C3) is strongly unstable so a question is how to quantitatively describe this instability. The anomalous cold air mass (C2) below the anomalous warm air mass (W2) is also another type of largely unstable situation to departure away from the temporal climatic state. Dynamically and horizontally, the anomalous warm air mass (W3) and the anomalous cold air mass (C2) were adjacently located nearby in the troposphere which possessed a large amount of anomalous potential energy (APE). The release of these APEs could produce strong anomalous kinetic energy (AKE) with ascending flow (green dashed contour) in the anomalous warm side and descending flow (green solid contour) in the anomalous cold side (Fig. 2c). The strongest contrast of anomalous warm-cold air masses and anomalous ascending-descending flows were around the place of tornadic storm and heavy rainfall. This vertical structure of height and temperature anomalies still remained but became weaker at 0600 UTC 28 Apr (Fig. 2c4). This vertical pattern of anomalous warm and cold air masses as well as negative and positive centers

of height anomalies in the central United States is the same as that in the single-tornado events occurred in eastern China (Qian et al. 2017a).

The vertical pattern of height and temperature anomalies, with a pair of anomalous height centers (L2 and H3) at the upper troposphere and the anomalous low (Lt) near the surface, persisted from 1200 UTC to 1800 UTC 27 Apr and 0000 UTC 28 Apr 2011. The strengthening process before 0000 UTC 28 Apr 2011 is evident in the rising flow shown in Fig. 2c. Thus, we assume that most strong tornadoes or supercell storms occurred from 1800 UTC 27 to 0000 UTC 28 Apr 2011 was a dynamical result releasing APE (reducing horizontal and vertical gradients of temperature anomalies), which transforms AKE to the anomalous rising flow in the mid-low troposphere. Therefore, the prediction of this vertical pattern of temperature-height anomalies should be relevant to that of severe weather events such as tornadic storm.

For this tornadic storm, we also examine its spatial distributions of specific humidity anomalies. Figure 3a shows the total and climatic specific humidity at the moment of a lot of tornado touchdowns at 0000 UTC 28 Apr 2011 along 38ºN. High specific humidity spans from east to west in the lower troposphere (Fig.3a). In Fig.3b, a positive center of specific humidity anomalies was just located over the surface low (Lt), within the places of tornado touchdown and heavy rainfall. So the tornado outbreak can be clearly indicated by a central place of specific humidity anomalies in the lower troposphere.

As we have previously noted, surface weather extremes are directly associated to variable anomalies aloft (Chen et al. 2016; Qian et al. 2016a; 2016b). Figure 4 illustrates the wind distributions at 0000 UTC 28 Apr 2011 from total, climatic, and anomalous components along 38ºN. In spring and over the central United States, prevailing climatic southwesterly (SW) flow exists in the upper troposphere and climatic northeasterly (NE) flow in the lower troposphere

(Fig. 4b). After removing the climatic wind from total wind (Fig. 4a), the residual wind shows that the tornado outbreak occurred in the boundary of anomalous southerly and northerly winds with strong rising flows in the troposphere (Fig. 4c).

The above case showed that a tornadic outbreak is directly associated with a vertically coupled variable anomalies deeply from the troposphere to the stratosphere. To confirm if this vertical air mass pattern can be generalized or not, we examine the 14 cases listed in Table 1. The first case occurred from 31 May to 1 Jun 1985. In Fig. 5, the horizontal distribution of height and temperature anomalies at 925 hPa was similar to that in Fig. 1c. There was no tornado touchdown at 1200 UTC 31 May 1985 (Fig. 5a), but a tornado was observed near the anomalous warm center (W1) at 1800 UTC 31 May 1985 (Fig. 5b). At 0000 UTC 1 Jun 1985, several tornadoes occurred within the anomalous warm center (W1) (Fig. 5c), while no tornadoes were recorded at 0600 UTC 1 Jun 1985 (Fig. 5d). For this case, the tornado outbreak was directly associated with a pair of anomalous cold-warm air masses (C and W1), but tornadoes occurred within the strengthening anomalous warm sector usually at 0000 UTC. The anomalous warm air mass (or warm sector) was located in the southeastern side of anomalous low center (L) and between two low troughs (two bold dashed lines) of height anomalies.

The eight cases of tornadic storm selected from Doswell et al. (2006) are illustrated in Fig. 6. Each of them had a multiple of tornadoes touched down simultaneously. Similar structures of height and temperature anomalies were also observed for other cases of tornadic storm, i.e. they are all associated with a pair of anomalous warm-cold air masses, and tornadoes occurred within warm side. These cases happened not only in spring (Mar, Apr and May), but also in the cold season (Nov and Dec). We find that all these cases showed the same vertical pattern of height and temperature anomalies.

Are there any differences in synoptic conditions between tornado and non-tornado severe events? Doswell et al. (2006) have ranked tornado and non-tornado environments, but they did not mention the horizontal distribution and vertical pattern of height and temperature anomalies for those non-tornadic severe storms. In this paper, we examine the 20 cases of the top-20 days with hail storms (Table 1) studied in Doswell et al. (2006b). The first case of hail storm was on 19 Jul 1983 but the hail sites were few compared to all 20 cases. Figs. 7 and 8 illustrate the height and temperature anomalies of the second and third cases of the hail days. Similar horizontal structures of anomalous warm-cold air masses and height anomalies at 925 hPa are observed from both of tornado and non-tornado (hail) cases, but vertical profiles are different from them, particularly for the depth of each air mass. For example, in the case from 8 to 9 Jun 1982, hail storms poured down near the boundary line of anomalous warm-cold air masses and the trough of height anomalies at 925 hPa (Figs.7a1–7a3). Therefore, the horizontal distribution of anomalous warm-cold air masses and height anomalies at the lower troposphere cannot distinguish tornado cases from non-tornado (hail) cases. Figure 7b reveals that although hail storms occurred near the boundary line of anomalous warm-cold air masses and the trough of height anomalies and within anomalous ascending flow in the lower troposphere, the center of anomalous warm or cold air mass was very shallow in depth so its intensity is weaker limited in the lower troposphere. Meanwhile, the central intensity of anomalous cold or warm air masses is also weaker at the upper troposphere. A comparison shows that the lower-layer anomalous warm air mass and upper-layer anomalous cold air mass are stronger for the tornado cases than that of hail cases (Fig. 2c vs. Fig. 7b).

In the case from 1800 UTC 7 Jun to 0600 UTC 8 Jun 1985, hail storm occurred only at the first two time points and near the boundary line of anomalous warm-cold air masses (W and C)

298 and the trough of height anomalies at 925 hPa (Fig. 8a). The weakening process of anomalous
299 warm-cold contrast is also observed in their horizontal and vertical sections in Fig. 8. This case
300 reconfirms that although the same horizontal distribution of height and temperature anomalies at
301 925 hPa is valid for both tornado and hail cases, their difference probably exists in the intensity
302 of vertical anomalous warm-cold air masses, which needs to be quantified.

303 All these cases showed that the spatial structure and expression are different between
304 traditional and anomalous synoptic charts in indicating the location of supercell tornadic and hail
305 storms. In the traditional synoptic charts, supercell storms move along or across air mass
306 boundaries such as warm fronts and stationary fronts as indicated by Schultz et al. (2014). It
307 means that the boundary of warm and cold air masses is divided by maximum temperature
308 gradient lines or fronts. In the anomalous synoptic charts, however, supercell storms are located
309 near the boundary of anomalous warm and cold air masses as well as within the places of higher
310 humidity anomalies and anomalous ascending flow (Fig. 2c, Fig. 3b and Fig. 10). It is noted that
311 tornado and hail outbreaks are anomalous weather events so they should well correspond to
312 anomalous weather systems as shown in Figs. 1c, 2c, 3b and 4c, and thus to the anomalous warm
313 and cold air masses in this study.

314

315 **4 Anomalous convective instability and comparison with other indices**

316 In the anomalous synoptic chart, anomalous warm and cold air masses observed are in synoptic
317 scale. For most tornado-producing storm systems such as in Fig. 2c panel, a pair of anomalous
318 warm-cold air masses (C2 and W3) horizontally spreads in the mid-low troposphere (below the
319 red dotted line) while another pair of anomalous warm-cold air masses (W2 and C3) penetrates
320 vertically from the upper troposphere to the stratosphere (above the red dotted line). Thus, two

pairs of adjacent anomalous air masses near tornado touchdown area are vertically deep from the troposphere to the stratosphere. When a cold anomaly lies above a warm anomaly it is defined as anomalous convectively unstable in the two deep layers. This spatial structure tells us that the traditional indices associated with the vertical temperature difference between 500 (or 600) and 850 hPa is not suitable to describe the instability of a pair of anomalous warm and cold air masses penetrated from the troposphere to the stratosphere. To quantitatively measure this structure of a pair of anomalous warm and cold air masses, the anomalous convective instability (*ACI*) index is defined as the difference of integrating temperature anomalies (*T'*) between two opposite air masses vertically at each grid point from 1000 to 100 hPa,

$$ACI = \left[\int T'dp\right]_{lower-layer} - \left[\int T'dp\right]_{upper-layer} \quad (3)$$

In the calculation of *ACI* index, the major anomalous warm and cold air masses are first identified by the vertically maximum and minimum centers of temperature anomalies such as the anomalous cold air mass (C2) versus the anomalous warm one (W2) or the anomalous warm air mass (W3) versus the anomalous cold one (C3) in Fig. 2c. Then, the temperature anomalies are vertically integrated within the anomalous warm (cold) air mass from the bottom +1ºC to the top +1ºC (or the bottom -1ºC to the top -1ºC) centering the maximum (or minimum) temperature anomaly (the vertical thick red or blue line in Figs. 2c4 or 7b1). The upper layer and the lower layer are vertically a pair of anomalous warm and cold air masses. For tornado cases, the two upper-layer anomalous air masses (W2 and C3) and the two lower-layer anomalous air masses (C2 and W3) are clearly separated by the zero-anomaly line (red-dot line in Figs. 2c), so are the non-tornado (hail) cases (Figs.7b and 8b).

Figure 9 shows the horizontal distributions of the ACI index at 1200 UTC 27, 1800 UTC 27, 0000 UTC 28, and 0600 UTC 28 Apr 2011, respectively. The horizontal gradient of ACI index

344 indicates the contrast of two pairs of anomalous warm and cold air masses. The total APE should
345 be directly proportional to the difference between the positive and negative ACIs. In Fig. 9, the
346 tornadoes touched down near the boundary between the positive and negative ACI areas but
347 within the positive area because of the anomalous ascending flow in Fig. 2c. The detail location
348 of tornadoes can also be determined by higher center of specific humidity anomalies and rising
349 flow (Figs. 2c and 3b) along the boundary of positive-negative ACI areas. The longest track with
350 most tornado touchdowns was associated to the strongest contrast of positive and negative ACI
351 areas with their central values of 10522 ºC hPa and -6729 ºC hPa respectively (Fig. 9c). Figure
352 10 shows the relation of tornado tracks associated with specific humidity and vertical flow at
353 four time points. Tornadoes touched down within higher humidity and rising flow. Tornadoes are
354 the most intense and touch down from other 14 tornado cases shown in Fig. 11. All 14 cases of
355 tornado outbreak happened near the boundary of positive and negative ACI areas or in the
356 positive ACI side, where the condition of specific humidity and wind anomalies was also
357 satisfied.

358 As a comparison, Fig. 12 is the horizontal distribution of ACI index calculated from the hail
359 storm cases shown in Figs. 7 and 8 at 0000 UTC 9 Jun 1982 and 0000 UTC 8 Jun 1985,
360 respectively. Hail storms also occur near the boundary between positive and negative ACI areas
361 but the contrast between the positive and negative ACI centers is weaker than that of the tornado
362 cases. Other 18 day cases show similar features as illustrated in Fig. 13. Most of the 20 hail day
363 cases showed weaker areas of ACI index except of several cases such as at 0000 UTC 21 Nov
364 1989 with only one hail site (Fig. 13k) and 0000 UTC 10 Apr 2001 with more hail sites (Fig.
365 13o). All cases of tornadic and hail storms occurred within anomalous high humidity and near
366 the boundary between positive and negative ACI areas. Most hail sites (16 of 20 cases) were

found in the positive ACI side and others in the negative side. In the triangle place as shown in Fig. 8b2, where ACI is negative due to the baroclinic structure of anomalous temperature-height system. The uncertainty of severe weather occurring in positive or negative ACI sides results from baroclinic system in anomalous variables. A comparison between tornado and hail cases (Table 1) shows that the ACI index of tornado cases is averagely about 1.5 times larger than that of hail storms: about 7355 ºC hPa to -8420 ºC hPa with their difference 15783 ºC hPa for the former and about 4808 ºC hPa to -5856 ºC hPa with their difference 10452 ºC hPa for the latter.

For the severe weather diagnostic analysis or forecasting, many indices have been developed in the last decades. Doswell and Schultz (2006) have given a selection of indices commonly used in the United States for severe storm forecasting. Most indices used in tornadic/non-tornadic storm detections are only associated with the vertical temperature difference or thermal wind between 500 (or 600) and 850 hPa in the lower troposphere. The updraft helicity (UH) is often used in the diagnostic analysis of strong convective weather events such as tornado outbreaks (Clark et al. 2013). An algorithm based on the concept of helicity, H, which is a scalar measure of potential for helicity flow (i.e., the pattern of a corkscrew) to develop in a moving fluid, was proposed by Kain et al. (2008). Rotating storms can be detected directly by measuring the vertical component of helicity, H_v, given by

$$H_v = w\left(\frac{\partial v}{\partial x} - \frac{\partial u}{\partial y}\right) = w\varsigma \cdot \tag{4}$$

Its vertical component H_v is integrated over a layer to yield a measure of the updraft helicity, UH, given by

$$UH = \int_{Zo}^{Zt} w\varsigma dz \tag{5}$$

388 The UH thus is calculated from 850 hPa (Z_o) to 500 hPa (Z_t) by (5). Figure 14 shows the
389 horizontal distributions of UHs and tornado tracks from 1200 UTC 27 to 0600 UTC 28 Apr 2011.
390 The anomalous rising flow (Fig. 2a) combined a positive vorticity anomaly (figures are not
391 shown) is a possible cause of severe weather. In Fig. 14, a positive center of UH was
392 accompanied with tornadic storms at 1200 UTC 27 Apr and then weakened and moved
393 northward to separate tornadic storms at 1800 UTC 27 Apr, 0000 UTC 28 and 0600 UTC 28 Apr
394 2011. This disadvantage showed that the positive UH center was weakened and moved away as
395 tornadic storm became stronger (Fig. 14). The UH is also used to calculate the two hail cases at
396 0000 UTC 9 Jun 1982 and 0000 UTC 8 Jun 1985 in Fig. 15. No signals of UH can indicate the
397 two hail occasions.

398 Convective available potential energy (CAPE) is an index commonly used in predicting
399 severe convective storms (Moncrieff and Miller 1976; Doswell and Rasmussen 1994). Generic
400 CAPE is calculated by integrating vertically the local buoyancy of a parcel from the level of free
401 convection (LFC) to the equilibrium level (EL). Mostly, the LFC and EL are respectively located
402 at around 800 and 600 hPa in the lower troposphere. Thus, CAPE is effectively the positive
403 buoyancy of an air parcel and is an indicator of atmospheric instability in the lower troposphere.
404 When an air mass is unstable, the warm air is displaced and accelerated upward by the ambient
405 air. This usually creates vertically-developed local clouds from convection, due to the rising
406 motion, which can sometimes lead to thunderstorms.

407 Usually, positive and high CAPE is an indicator to where convective weather events might
408 occur. Figures 16 and 17 show the horizontal distributions of CAPE for tornado and hail cases,
409 respectively, using the NARR data. It is noted that most tornadoes of the 14 cases occurred in the
410 northward moderate CAPE area rather than the high-value center of CAPE (Fig. 16). For the 20

411 hail days, the first shows that hail sites occurred in the northward moderate CAPE area far away
412 to the high CAPE center (Fig. 17a) while the second depicts that most hail sites occurred near the
413 high CAPE center (Fig. 17b). Similar relationship between hail occurrence and CAPE value can
414 be observed from other days in Fig. 17. This result suggests that although CAPE is a useful
415 indicator for severe convective weather events such as tornadic and hail storms but it cannot
416 distinguish tornado and non-tornado events as done by the *ACI* index.

417 Another index is the severe weather threat (SWEAT) index which evaluates the potential
418 for severe weather by combining several parameters into one index. The SWEAT index was
419 developed by Bidner (1970).

420 $$\mathbf{SWEAT=12[T_d(850hPa)]+20(TT-49)+2(f8)+f5+125(S+0.2)} \quad \mathbf{(6)}$$

421 It includes: 1) the low-level moisture (850 hPa dew point T_d in degree Celsius, if $T_d<0$, the term
422 is set to zero), 2) the instability (Total Totals Index, *TT* is the sum of the 850 hPa temperature
423 and dew point, minus twice the 500 hPa temperature, if $TT<49$, the term $20(TT-49)$ is set to
424 zero), 3) the wind speeds in knots at the 850 hPa (f8) and the 500 hPa (f5), and the wind shear
425 S=sin(wind direction difference by 500 hPa minus 850 hPa) under many conditions. The
426 SWEAT over 400 is potential for tornadic storms and the SWEAT values in between 300 and
427 400 indicate the threshold for severe thunderstorms and the SWEAT values in between 250 and
428 300 indicate a potential for strong convection in practice.

429 Figure 18 shows the distributions of SWEAT index at 1200 UTC 27, 1800 UTC 27, 0000
430 UTC 28, and 0600 UTC 28 Apr 2011. Most tornado tracks occurred in northeast side of the
431 region with SWEAT over 400 in the first two time points and they were locally accompanied
432 well with one of SWEAT centers in the last two time points, where anomalous high humidity
433 was located (Fig. 10). In Fig. 18, there are other several centers of SWEAT without tornado

appearance. In Fig. 19, one stronger center of SWEAT over 400 accompanied scattering hail sites at 0000 UTC 9 Jun 1982 while one weaker SWEAT center at 0000 UTC 8 Jun 1985 shows many hail sites in its southwest side.

It is clear that all these indices the SWEAT, UH and CAPE used air temperature, dew point and wind are limited in the lower troposphere between 500 and 850 hPa. In all three indices, the SWEAT considering the low-level moisture and wind shear is better than others to indicate the locations of potential weather extreme but they cannot distinguish tornadic and hail storms. As in Fig. 2c and Fig. 7b, the layer between 500 and 850 hPa is located within only an anomalous air mass. It implies that traditional indices cannot deeply reflect the strong contrast of two opposite anomalous air masses to indicate a potential weather extreme such as tornadic and hail storms.

5. Conclusions and discussion

This paper first clarified that the spatial structure and expression are different from traditional and anomalous synoptic charts in indicating the location of tornadic and hail storms. In the traditional synoptic charts, supercell storms are considered to move along or across the warm and stationary fronts where a maximum temperature gradient line is further considered as the boundary of warm and cold air masses (Schultz et al. 2014). In the anomalous synoptic charts, however, supercell storms are located near the boundary of anomalous warm and cold air masses, and within the places of higher humidity anomalies and anomalous ascending flow. By using the anomalous synoptic charts, we can construct the internal relation between the surface weather extremes and spatial pattern of anomalous variables. Horizontal and vertical structures cannot be found in the traditional synoptic charts (Fig. 1a, Fig. 2a and Fig. 3a), but spatial structures of all anomalous variables connecting to the surface weather extremes become clear in the anomalous

457 synoptic charts (Fig. 1c, Fig. 2c, Fig. 3b, Fig. 7 and Fig. 8). This means that the anomaly-based
458 method is clearer and less confusing to locate the surface weather extremes than the traditional
459 way. These spatial structures or patterns can be used by forecasters in practical extreme weather
460 recognition based on observations and medium-range model products in the future.

461 Through case analyses we conclude the notion that tornadic and hail storms are directly related
462 to the vertical pattern of anomalous warm and cold air masses revealed in anomalous synoptic
463 chart. The appearance of two horizontal adjacent high and low centers of height anomalies at the
464 upper troposphere as well as two pairs of adjacent anomalous warm and cold centers (or air
465 masses) from the troposphere to the stratosphere are the critical environmental elements
466 producing severe weather including tornadic and non-tornadic storms. Horizontally, tornado
467 outbreaks usually occur near the boundary between anomalous warm and cold air masses, and
468 mostly within anomalous warmer and moister updraft air mass in the mid-low troposphere.
469 Vertically, an anomalous cold air mass located above an anomalous warm air mass produces the
470 instability necessary for intense convective storms. Thus, a pair of strong adjacent anomalous
471 warm and cold air masses horizontally in the troposphere is favorable for the release of
472 anomalous potential energy to produce anomalous kinetic energy. The tornado outbreak is
473 associated with a pattern of two pairs of adjacent synoptic-scale centers of temperature
474 anomalies horizontally and by a vertical pattern of anomalous warm-cold air masses from the
475 troposphere to the stratosphere.

476 This horizontal structure and vertical pattern of height and temperature anomalies are suitable
477 for both tornadic and hail storms. But, the intensity and contrast of two pairs of adjacent warm-
478 cold air masses for hail storms are usually weaker. Thus, we defined an ACI index: the
479 difference of two anomalous warm and cold air masses vertically from the troposphere to the

480 stratosphere. The ACI index can be physically considered as the storage of anomalous potential
481 energy to generate severe weather. It is found that the ACI intensity of tornado-producing storm
482 is about 1.5 times larger than that of hail-producing storm. In most strong cases, tornadic and hail
483 storms usually occur in the side of anomalous warm air mass with anomalous high humidity and
484 ascending flow. Sometimes they are located in the side of anomalous cold air mass due to some
485 baroclinic systems of height and temperature anomalies from the troposphere to the stratosphere.
486 The ACI index is different from the traditional instability indices such as the UH, CAPE and
487 SWEAT, whose are vertically limited within the mid-low troposphere, usually in the layer
488 between 500 and 850 hPa. This limitation and case analysis indicated that the three indices
489 cannot distinguish tornadic and hail storms.

490 This paper shows the advantages of anomaly-based approach in analyzing severe storm
491 environment. The anomalous variables can be used to plot anomalous synoptic charts (Qian et al.
492 2014) and construct diagnostic indices (Qian et al. 2016b) like the ACI index. In this study, for
493 example, by using the anomalous synoptic chart, severe weather storms have been proved to
494 result from the contrast between anomalous warm-wet and cold-dry air masses. In practice, many
495 approaches already exist to get a "quick look" for the potential of severe weather (Doswell and
496 Schultz, 2006). In this study, however, the analysis is not sufficient to categorically prove the
497 superiority of ACI index in predicting when and where tornadic or hail storms will occur. To
498 make this conclusion genuinely robust, the verification from more tornado cases and non-tornado
499 days is still needed, but the current paper can serve as a starting point.

500 Finally, the pattern of two pairs of adjacent warm-cold centers and the ACI index derived from
501 the anomaly-based analysis allow forecasters to detect severe weather events, and possibly to
502 distinguish tornado outbreaks and non-tornadic storm events if a critical threshold can be found

in future research statistically based on more cases, and use them as a guide in making their prediction of tornado outbreak and hail storm. This method can also be applied to the products of meso-scale numerical model predictions of 24–36 hours to serve as early anomaly signals leading to tornadic outbreak and hail storm at early time. This utility certainly relies on the model ability to accurately predict the presence of those anomalies.

Acknowledgements

The authors are very grateful for the constructive comments from the two anonymous reviewers and editor, which were crucial to improving this manuscript. This work is supported by the National Natural Science Foundation of China (41375073 and 41775067).

References

Agee E, Church C, Morris C, Snow J (1975) Some synoptic aspects and dynamic features of vortices associated with the tornado outbreak of 3 April 1974. Mon. Wea. Rev. 103(4):318–333

Bidner, A (1970) The AFGWC Severe Weather Threat Index: A Preliminary Report. AWS TR242: 229-231

Bunkers MJ, Johnson JS, Czepyha LJ, Grzywacz JM, Klimowski BA, Hjelmfelt MR (2006) An

524 observational examination of long-lived supercells. Part II: Environmental conditions and
525 forecasting. Wea. Forecasting 21(5):689–714
526 Chen Y, Hu Q, Yang YM, and Qian WH (2016) Anomaly-based analysis of extreme heat waves
527 in Eastern China during 1981–2013. Int. J. Clim. 37(1): 509–523
528 Corfidi S, Weiss S, Kain J, Corfidi S, Rabin R, Levit J (2010) Revisiting the 3–4 April 1974
529 Super Outbreak of tornadoes. Wea. Forecasting 25(2):465–510
530 Dee DP, Coauthors (2011) The ERA-Interim reanalysis: Configuration and performance of the
531 data assimilation system. Quart. J. R. Meteorol. Soc. 137(656):553–597
532 Doswell CA, Rasmussen EN (1994) The effect of neglecting the virtual temperature correction
533 on CAPE calculations. Wea. Forecasting **9** (4): 625–9
534 Doswell CA, Schultz DM (2006a) On the use of indices and parameters in forecasting severe
535 storms. Electronic J. Severe Storms Meteor 1(3): 1–22
536 Doswell CA, Edwards R, Thompson RL, Hart JA, Crosbie KC (2006b) A simple and flexible
537 method for ranking severe weather events. Wea. Forecasting 21(6):939–951
538 Doswell CA, Carbin GW, Brooks HE (2012) The tornadoes of spring 2011 in the USA: An
539 historical perspective. Weather 67(4): 88–94
540 Glickman TE (2000) Glossary of Meteorology. 2nd ed. Amer. Meteor. Soc. pp 855
541 Huang J, Du J, Qian WH (2015) A comparison between Generalized Beta-Advection Model and
542 classical Beta-Advection Model in predicting and understanding unusual typhoon tracks in
543 eastern China seas. Wea. Forecasting 30(3):771-92
544 Jiang N, Qian WH, Du J, Grumm RH, Fu JL (2016) A comprehensive approach from the raw
545 and normalized anomalies to the analysis and prediction of the Beijing extreme rainfall on
546 July 21, 2012. Natural Hazards 84(3):1551–1567

547 Joyce RJ, Janowiak JE, Arkin PA, Xie PP (2004) Cmorph: a method that produces global
548 precipitation estimates from passive microwave and infrared data at high spatial and
549 temporal resolution. J. Hydrometeor 5(3):487−503
550 Knupp et al. (2014) Meteorological overview of the devastating 27 April 2011 tornado outbreak.
551 Bull. Amer. Meteor. Soc. 95(7):1041−1062
552 Mercer AE, Shafer CM, Doswell CA, Leslie LM, Richman MB (2012) Synoptic composites of
553 tornadic and nontornadic outbreaks. Mon. Wea. Rev. 140: 2590–2608
554 Metz N, Bosart L (2010) Derecho and MCS development, evolution, and multiscale interactions
555 during 3–5 July 2003. Mon. Wea. Rev. 138(8):3048–3070
556 Moncrieff MW, Miller MJ (1976) The dynamics and simulation of tropical cumulonimbus and
557 squall lines. Q. J. R. Meteorol. Soc. 120 (432): 373–94
558 Qian WH, Li J, Shan XL (2013) Application of synoptic-scale anomalous winds predicted by
559 medium-range weather forecast models on the regional heavy rainfall in China in 2010. Sci.
560 China Earth Sci. 56(6):1059–1070
561 Qian WH, Shan XL, Liang HY, Huang J, Leung JCH (2014) A generalized beta advection model
562 to improve unusual typhoon track prediction by decomposing total flow into climatic and
563 anomalous flows. J. Geophys. Res. Atmos. 119(3):1097–1117
564 Qian WH, Chen Y, Jiang M, Hu Q (2015) An anomaly-based method for identifying signals of
565 spring and autumn low temperature events in the Yangtze River Valley, China. J. Appl.
566 Meteorol. Climatol. 54(6):1216-1233
567 Qian WH, Jiang N, Du J (2016a) Anomaly based weather analysis vs. traditional total-field
568 based weather analysis for depicting regional heavy rain events. Wea. Forecasting
569 31(1):71–93

570 Qian WH, Yu TT, Du J (2016b) A unified approach to trace surface heat and cold events by
571 using height anomaly. Clim. Dyn. 46(5):1647–1664
572 Qian WH, Leung JCH, Jin RH, Fu JL, Wu FF, Kuang ZJ, Du J (2017a) Application of
573 anomalous variables in severe convection system analyses and model evaluation: A case
574 study on tornado-producing anomalous systems near Lixiahe basin, Jiangsu Province.
575 Meteorol. Mon. 43(2):129–143
576 Qian WH, Huang J (2017b) Impact of different climatic flows on typhoon tracks. Meteorol.
577 Atmos. Phys. doi: 10.1007/s00703-017-0515-z
578 Qian WH (2017c) Temporal Climatology and Anomalous Weather Analysis, Springer
579 Atmospheric Sciences, doi: 10.1007/978-981-10-3641-5_2
580 Schaefer JT, Edwards R (1999) The SPC tornado/severe thunderstorm database. Preprints, 11th
581 Conf. on Applied Climatology, Dallas, TX, Amer. Meteor. Soc. 603–606.
582 Schultz DM, Richardson YP, Markowski PM, Doswell CAIII (2014) Tornadoes in the Central
583 United States and the “Clash of Air Masses”. Bull. Amer. Meteorol. Soc. 95(11):1704-1712.
584 Simmons KM, Sutter D (2012) The 2011 tornadoes and the future of tornado research. Bull.
585 Amer. Meteorol. Soc. 93(7):959–961
586 Thompson RL, Edwards R (2000) An overview of the environmental conditions and forecast
587 implications of the 3 May 1999 tornado outbreak. Wea. Forecasting 15(6):682–699
588 Verbout SM, Brooks HE, Leslie LM, Schultz DM (2006) Evolution of the U.S. tornado database:
589 1954–2003. Wea. Forecasting 21(1):86–93
590 Clark A J, Gao JD, Marsh PT, Smith T, Kain JS, Jr JC, Xue M, and Kong FY. 2013. Tornado
591 Pathlength Forecasts from 2010 to 2011 Using Ensemble Updraft Helicity. *Wea.*
592 *Forecasting,* **28,** 387–407.

593 Kain, J. S., S. J. Weiss, D. R. Bright, M. E. Baldwin, J. J. Levit, G. W. Carbin, C. S. Schwartz,
594 M. L. Weisman, K. K. Droegemeier, D. B. Weber, K. W. Thomas, 2008: Some practical
595 considerations regarding horizontal resolution in the first generation of operational
596 convection-allowing NWP. *Wea. Forecasting,* **23(5),** 931–952.

597 Mesinger,F., and Coauthors, 2006: North American Regional Reanalysis. *Bull. Amer. Meteor.*
598 *Soc.*,**87,** 343–360.

599

600

601

602

603

604

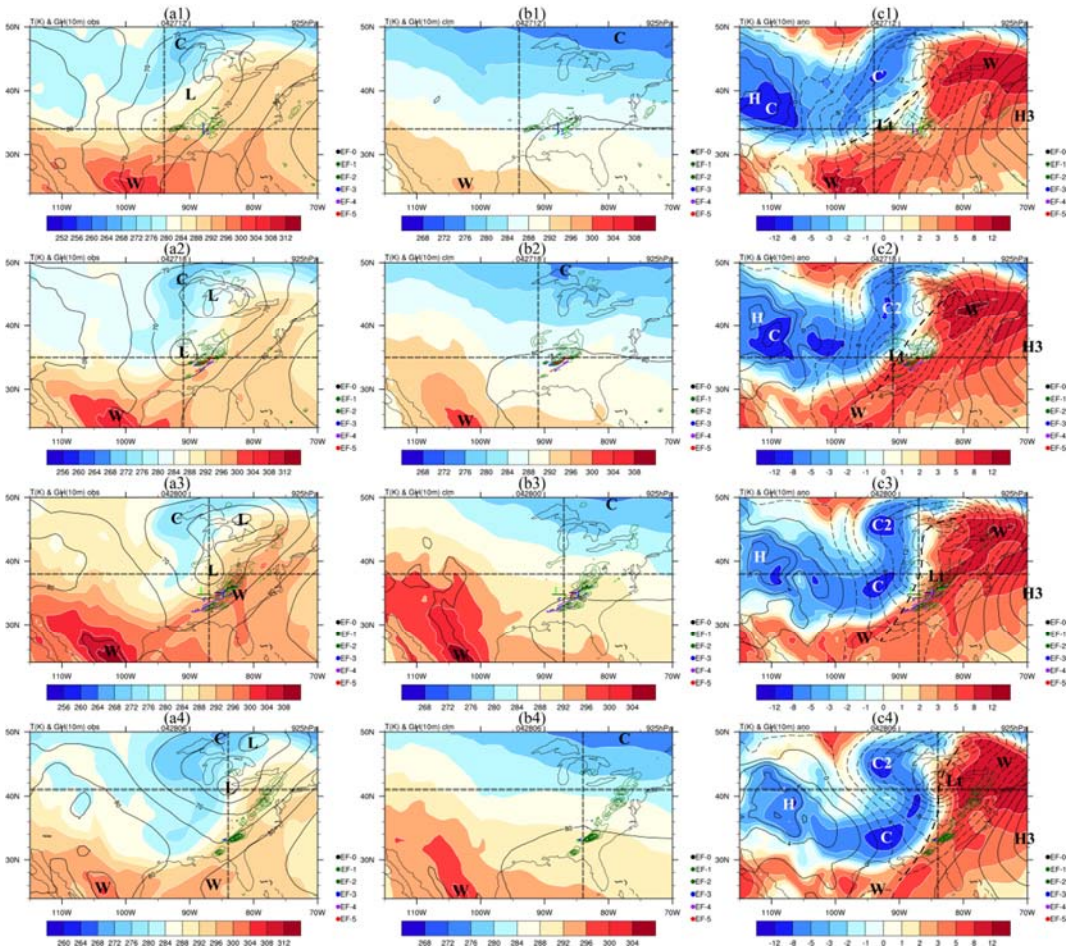

Figure 1. Horizontal distributions of (a1) total height (contour, 5×10 gpm interval) and total temperature (shading, 4 K interval), (b1) climatic height (contour, 5×10 gpm interval) and climatic temperature (shading, 4 K interval), and (c1) height anomalies (contours, 2×10 gpm interval) and temperature anomalies (shading, 1, 2, 3 and 4K intervals) at 925 hPa at 1200 UTC 27 Apr 2011. Similarly, panels (a2)–(c2) are at 1800 UTC 27, (a3)–(c3) at 0000 UTC 28, and (a4)–(c4) at 0600 UTC 28 Apr 2011. Green contour indicates the hourly precipitation rate (2.5 mm h^{-1} interval) and the thick dashed line in (c) denotes the trough of height anomalies. Colored straight lines denote tornado tracks from EF-0 to EF-5 scales centered within 6 hours. Letters "H/L" and "W/C" indicate the centers of height and temperature (or anomalies).

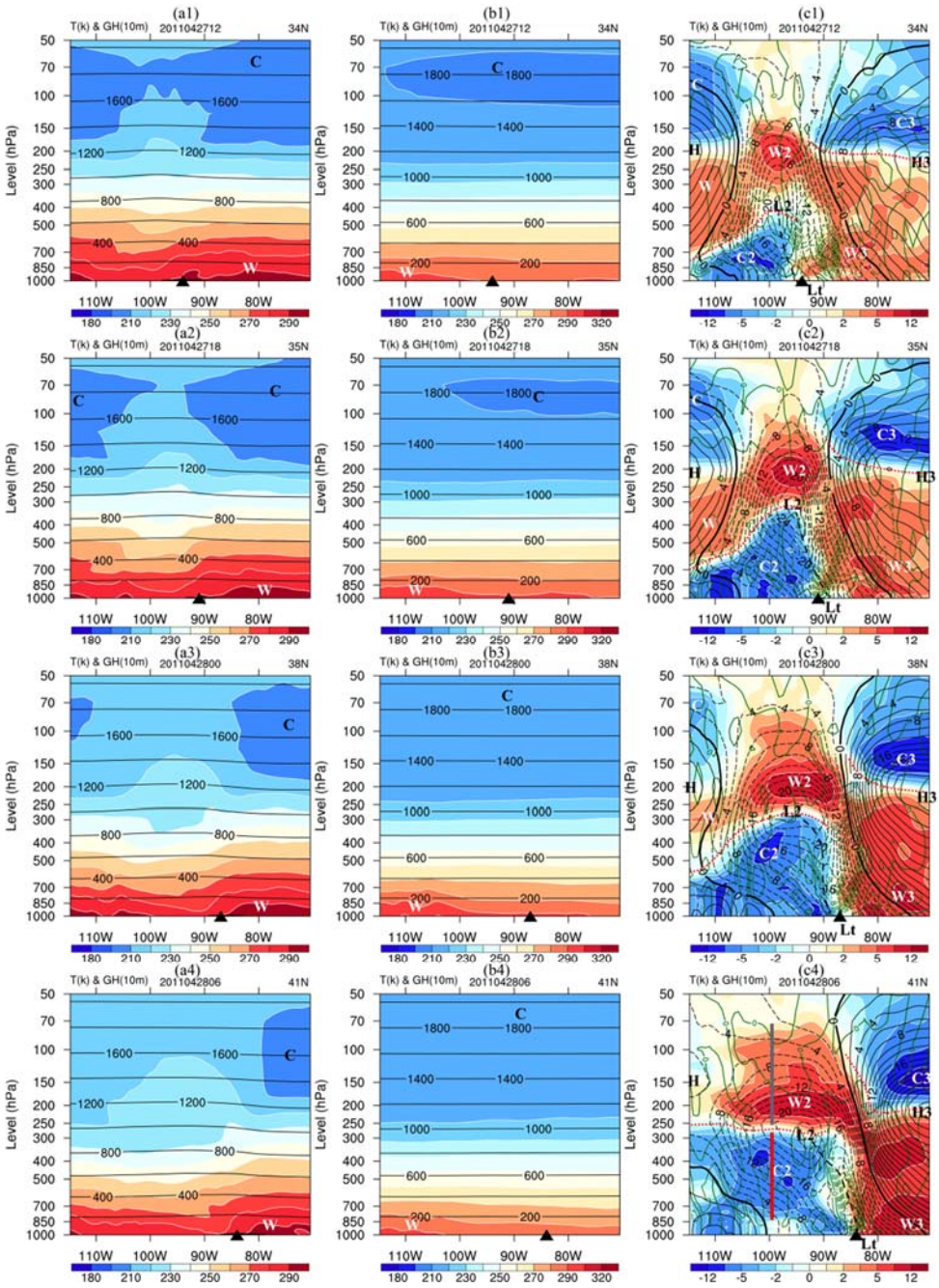

Figure 2. Vertical distributions of (a1) total height (contour, 200×10 gpm interval) and total temperature (shading, 10 K interval), (b1) climatic height (contour, 200×10 gpm interval) and climatic temperature (shading, 10 K interval), and (c1) height anomalies (contours, 2×10 gpm interval) and temperature anomalies (shading, 1, 1.5, and 3.5K intervals) along 34ºN at 1200 UTC 27 Apr 2011. Similarly, panels (a2)–(c2) are along 35ºN at 1800 UTC 27 Apr 2011, (a3)–(c3) along 38ºN at 0000 UTC 28 Apr 2011, and (a4)–(c4) along 41ºN at 0600 UTC 28 Apr 2011. The filled triangle "▲" indicates the central position of the surface anomalous low (Lt), while thick dashed lines indicate the trough axis of height anomalies. The green solid and dashed

628 contours respectively indicate anomalous sinking and rising pressure velocities (0.2 Pa s^{-1}
629 interval) while the red-dot line is the zero line of temperature anomalies in (c). Letters "H/L" and
630 "W/C" denote the centers of height and temperature (or anomalies). In (c4), the vertical thick red
631 and blue lines denote the depths (lower-layer or higher-layer) of anomalous warm (over +1°C)
632 and cold (below -1°C) air masses, respectively.

633

634

635

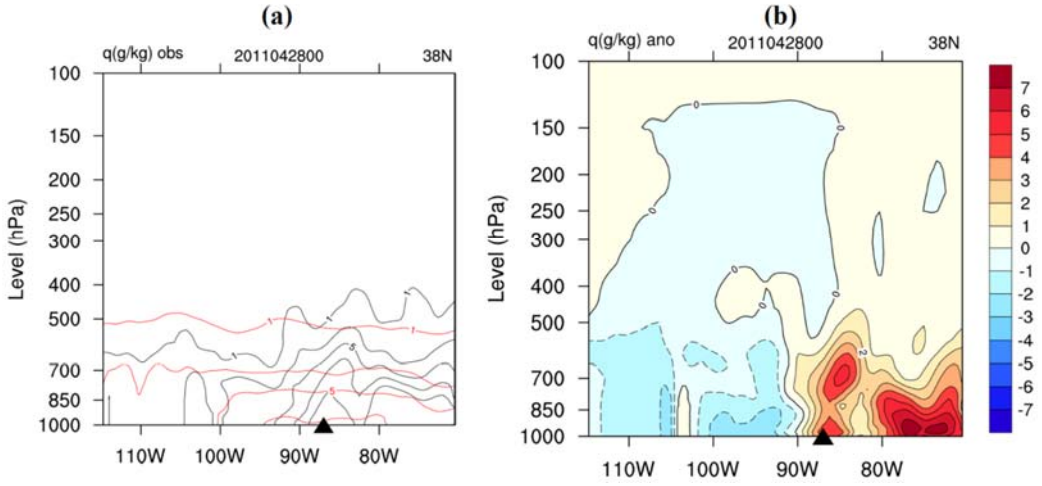

636

637 **Figure 3.** Vertical distributions of specific humidity at 0000 UTC 28 Apr 2011 for (a) total
638 specific humidity (black contours, 2 g/kg interval) and climatic specific humidity (red contours,
639 2 g/kg interval) and (b) specific humidity anomalies (shading, 1g/kg interval) along 38°N. The
640 filled triangle "▲" indicates the central position of the surface anomalous low (Lt) near the place
641 of tornado touchdowns and heavy rainfall.

642

643

644

645

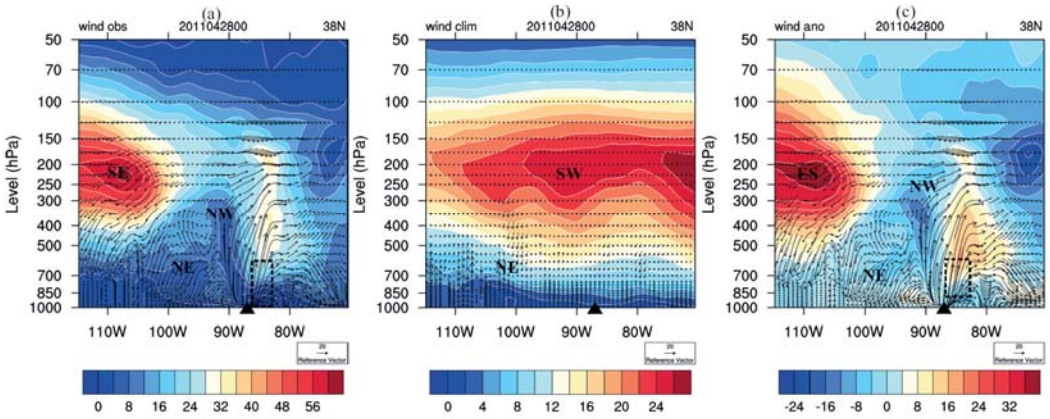

Figure 4. Vertical distributions of wind (m/s) at 0000 UTC 28 Apr 2011 for (a) total wind, (b) climatic wind, and (c) wind anomaly along 38ºW. Red and blue shadings are southerly and northerly velocities. The dashed box is the place of tornado touchdowns and heavy rainfall. The vertical velocity has been amplified 100 times. Letters "SW", "ES", "NW" and "NE" indicate the southwesterly, southeasterly, northwesterly and northeasterly flows respectively. The filled triangle "▲" indicates the central position of the surface anomalous low (Lt).

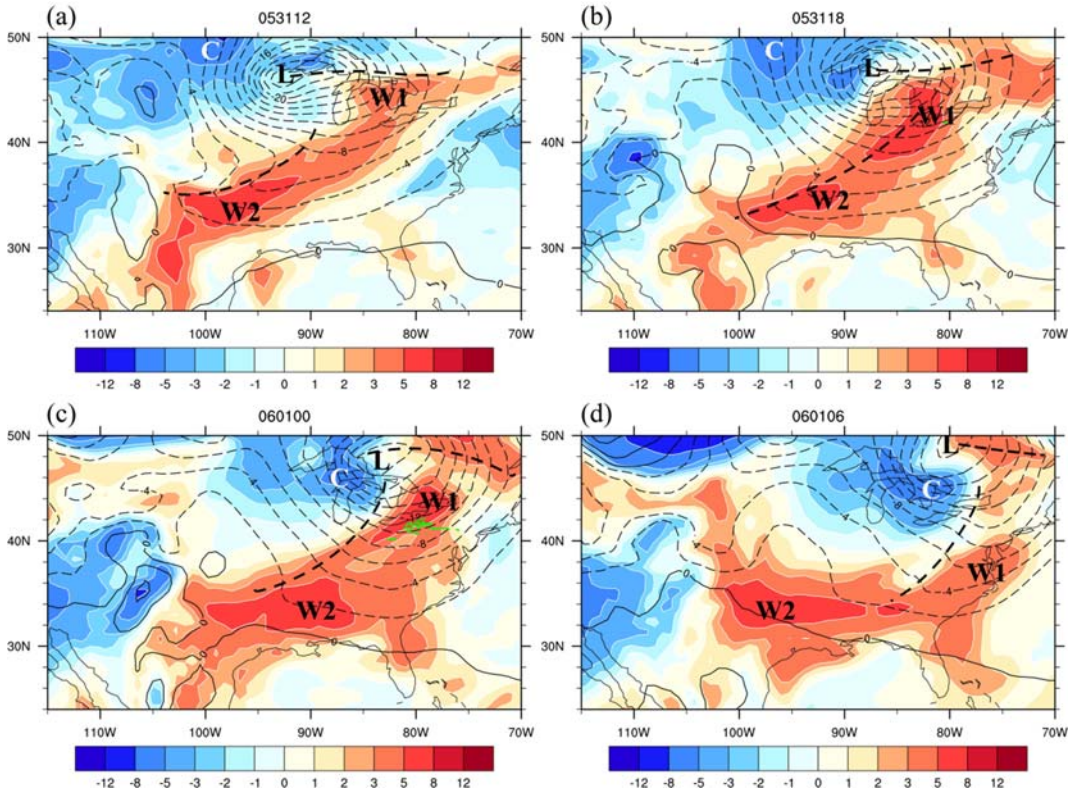

Figure 5. Horizontal distributions of height anomalies (contours, 2×10 gpm interval) and temperature anomalies (shading, 1, 2, 3 and 4K intervals) at 925 hPa at (a) 1200 UTC 31 May, (b) 1800 UTC 31 May, (b) 0000 UTC 1 Jun, and (d) 0600 UTC 1 Jun 1985. Green stars and lines are locations and tracks of tornadoes centered within 6 hours. The bold dashed line denotes the trough of height anomalies.

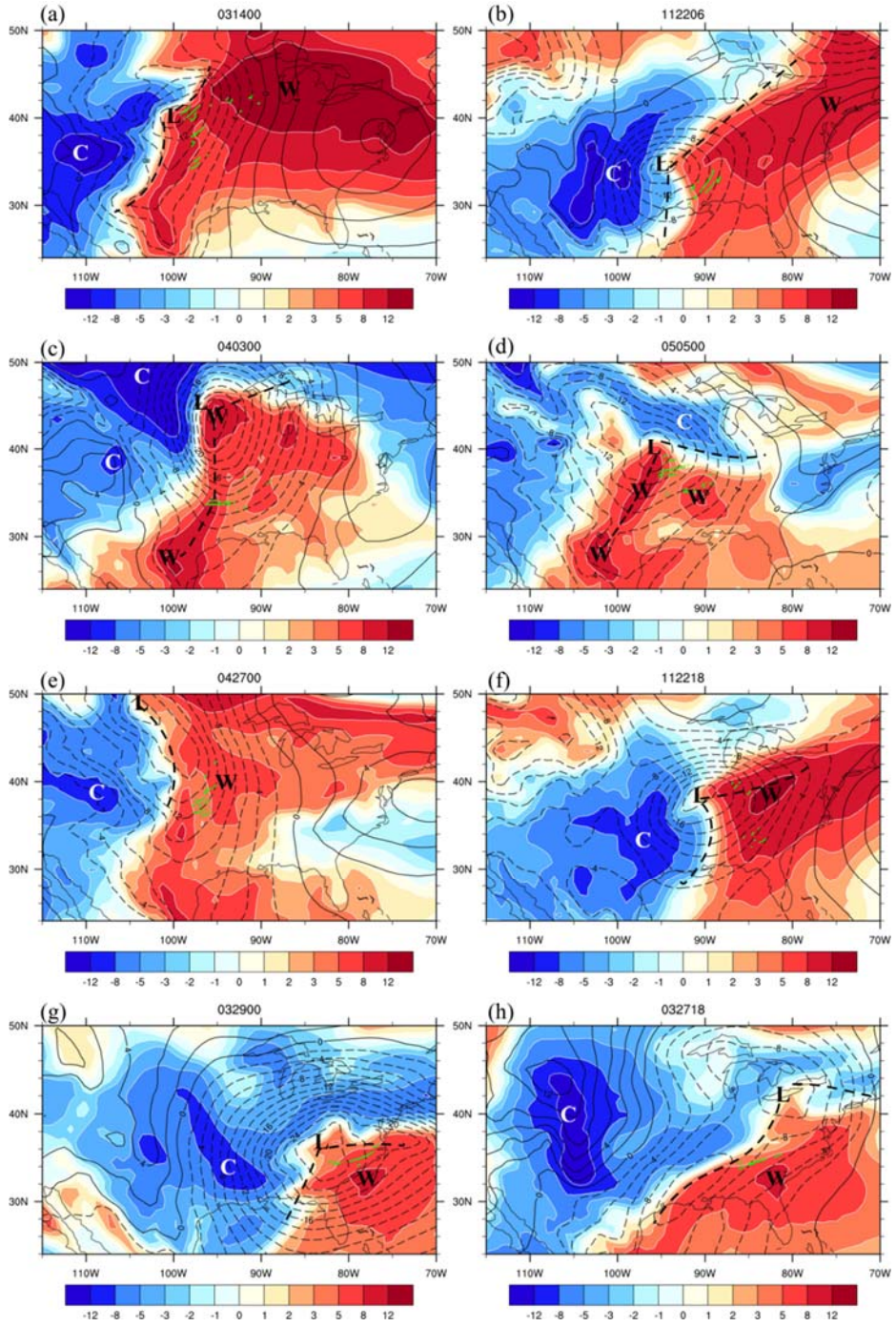

672

673 **Figure 6.** Same as Fig. 5 except at (a) 0000 UTC 14 Mar 1990, (b) 0600 UTC 22 Nov 1992, (c)
674 0000 UTC 3 Apr 1982, (d) 0000 UTC 5 May 2003, (e) 0000 UTC 27 Apr 1991, (f) 1800 UTC 22
675 Nov 1992, (g) 0000 UTC 29 Mar 1984, (h) 1800 UTC 27 Mar 1994, when many tornadoes
676 touched down.

677

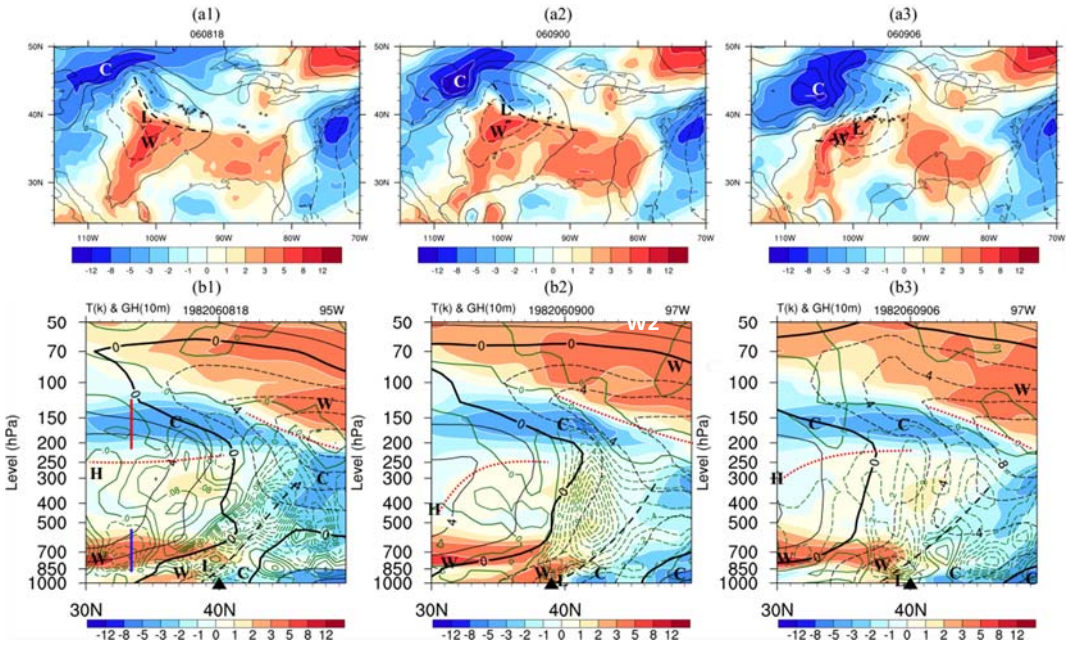

Figure 7. The upper panel is the same as Fig. 1c except at (a1) 1800 UTC 8, (a2) 0000 UTC 9, and (a3) 0600 UTC 9 Jun 1982. The lower panel is the same as Fig. 2c except at (a1) 1800 UTC 8 along 95°W, (a2) 0000 UTC 9 along 97°W, and 0600 UTC 9 Jun 1982 along 97°W. Small stars in (a) are locations of hails centered within 6 hours. The filled triangle "▲" in (b) indicates the central position of hail storms. The green solid and dashed contours in (b) respectively indicate anomalous sinking and rising pressure velocities (0.2 Pa s^{-1} interval). In (b1), the vertical thick red and blue lines denote the depths (lower-layer or higher-layer) of anomalous warm (over +1°C) and cold (below -1°C) air masses, respectively.

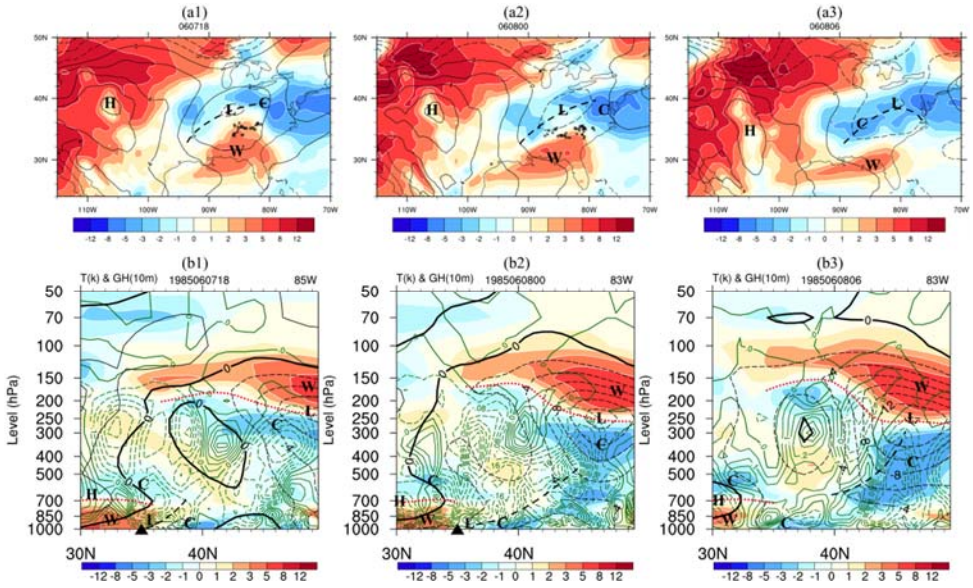

Figure 8. Same as Fig.7 except at 1800 UTC 7, 0000 UTC 8, and 0600 UTC 8 Jun 1985.

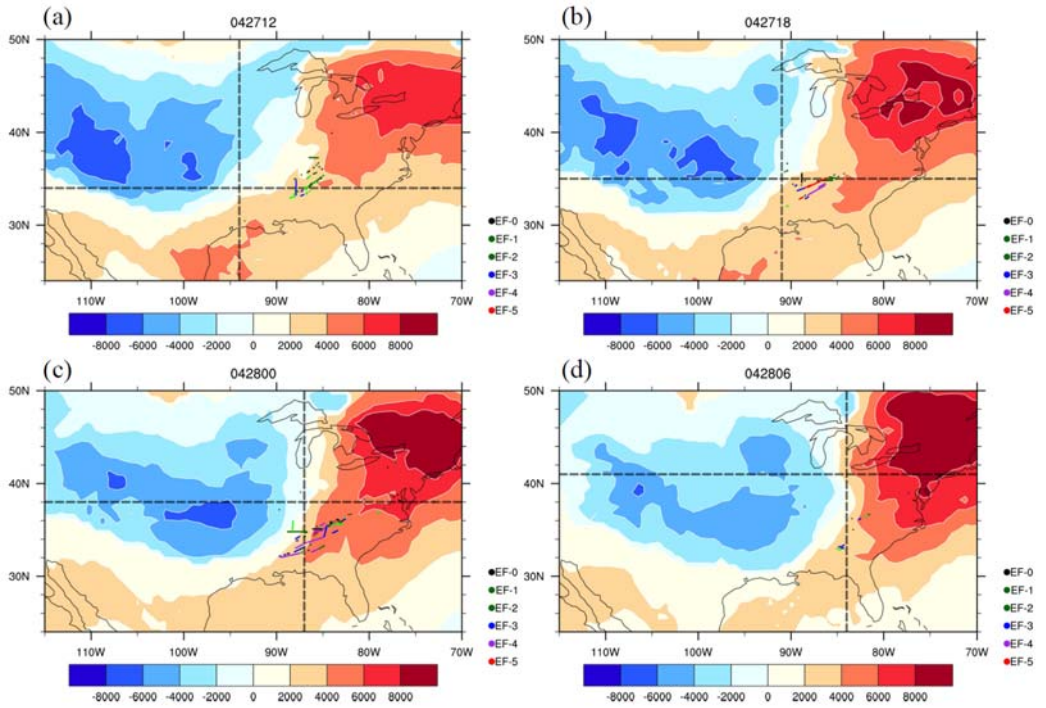

Figure 9. Same as Fig. 1c except of horizontal distributions of the *ACI* index (shading, 2000ºC interval) at (a) 1200 UTC 27, (b) 1800 UTC 27, (c) 0000 UTC 28, and (d) 0600 UTC 28 Apr 2011.

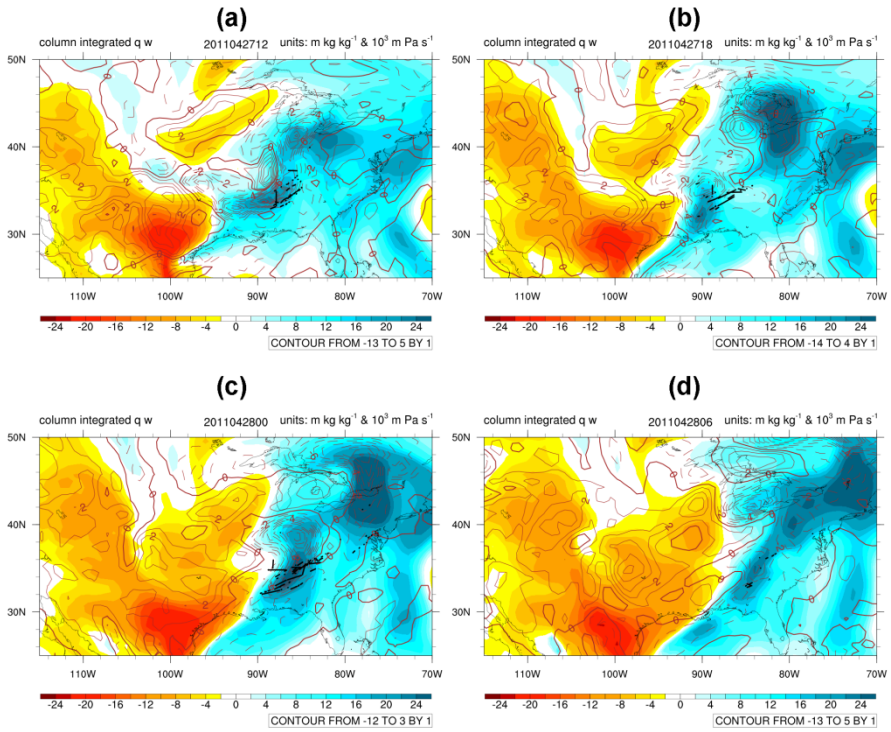

705

706 **Figure** 10. Same as Fig. 9 except of horizontal distributions of the 500–1000hPa column
707 integrated specific humidity (shading, 2 m kg kg^{-1} interval) and 300–1000hPa column integrated
708 vertical velocity (contour, 10^{-3} m Pa s^{-1} interval) and at (a) 1200 UTC 27, (b) 1800 UTC 27, (c)
709 0000 UTC 28, and (d) 0600 UTC 28 Apr 2011.

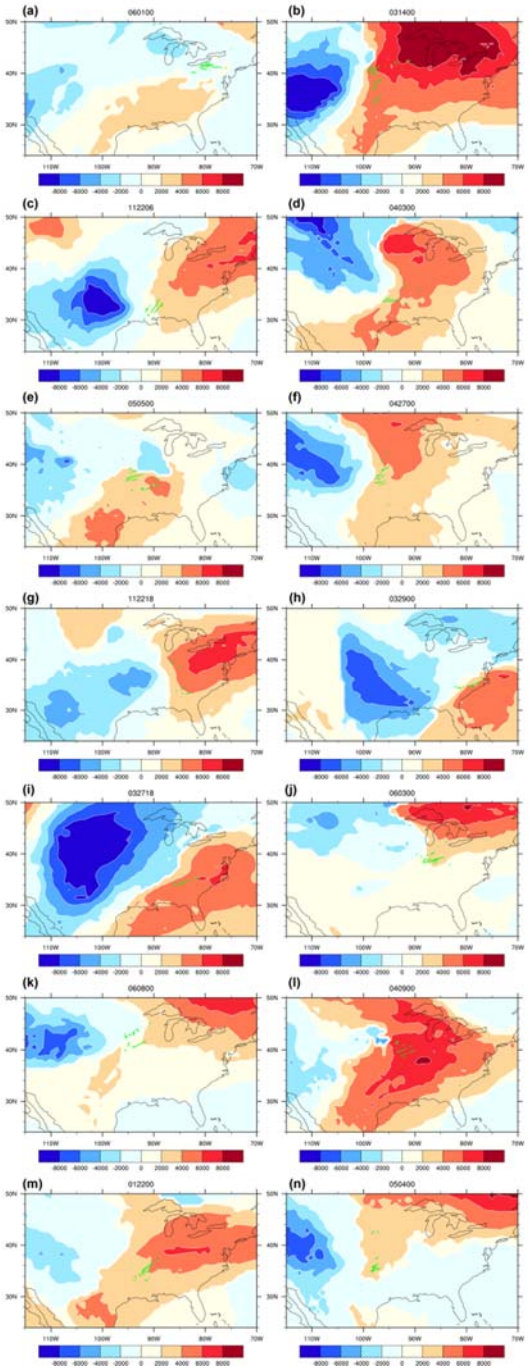

710

711 **Figure 11.** Same as Fig. 9 except at (a) 0000 UTC 1 Jun 1985, (b) 0000 UTC 14 Mar 1990, (c)
712 0600 UTC 22 Nov 1992, (d) 0000 UTC 3 Apr 1982, (e) 0000 UTC 5 May 2003, (f) 0000 UTC
713 27 Apr 1991, (g) 1800 UTC 22 Nov 1992, (h) 0000 UTC 29 Mar 1984, (i) 1800 UTC 27 Mar
714 1994, (j) 0000 UTC 3 Jun 1990, (k) 0000 UTC 8 Jun 1984, (l) 0000 UTC 9 Apr 1999, (m) 0000
715 UTC 22 Feb 1999, (n) 0000 UTC 4 May 1999.

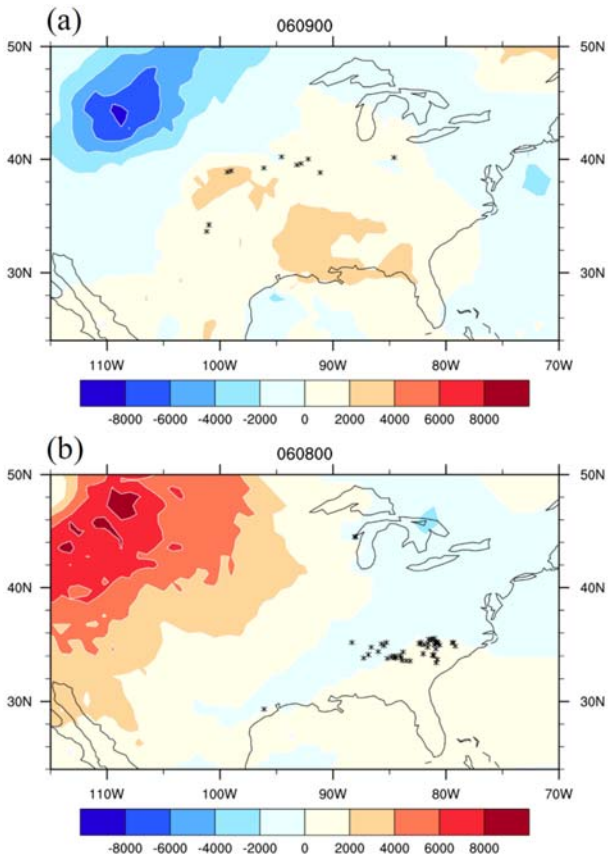

716

717 **Figure 12.** Same as Fig. 9 except at (a) 0000 UTC 9 Jun 1982 and (b) 0000 UTC 8 Jun 1985.
718 Black stars are locations of hail centered within 6 hours.

719

720

721

722

723

724

725

726

727

728

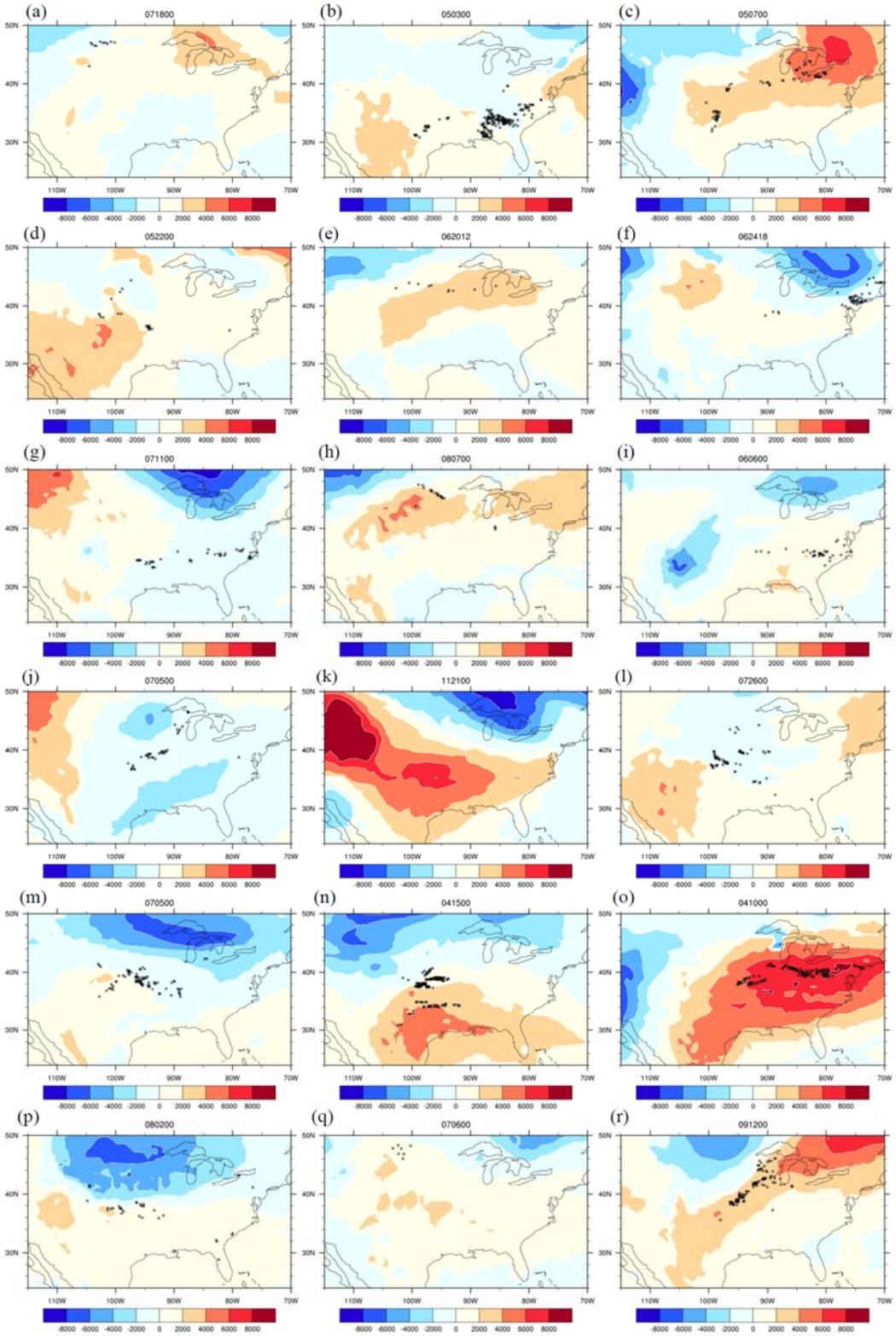

729

730 **Figure 13.** Same as Fig. 9 except for hail storms at (a) 0000 UTC 18 Jul 1983, (b) 0000 UTC 3
731 May 2003, (c) 0000 UTC 7 May 1986, (d) 0000 UTC 22 May 1989, (e) 1200 UTC 20 Jun 1997,

(f) 1800 UTC 24 Jun 1985, (g) 0000 UTC 11 Jul 1985, (h) 0000 UTC 7 Aug 1980, (i) 0000 UTC 6 Jun 1985, (j) 0000 UTC 5 Jul 1985, (k) 0000 UTC 21 Nov 1989, (l) 0000 UTC 26 Jul 1995, (m) 0000 UTC 5 Jul 1992, (n) 0000 UTC 15 Apr 2001, (o) 0000 UTC 10 Apr 2001, (p) 0000 UTC 2 Aug 1986, (q) 0000 UTC 6 Jul 1980, and (r) 0000 UTC 12 Sep 2000. In (k), one star is near 40ºN and 75ºW.

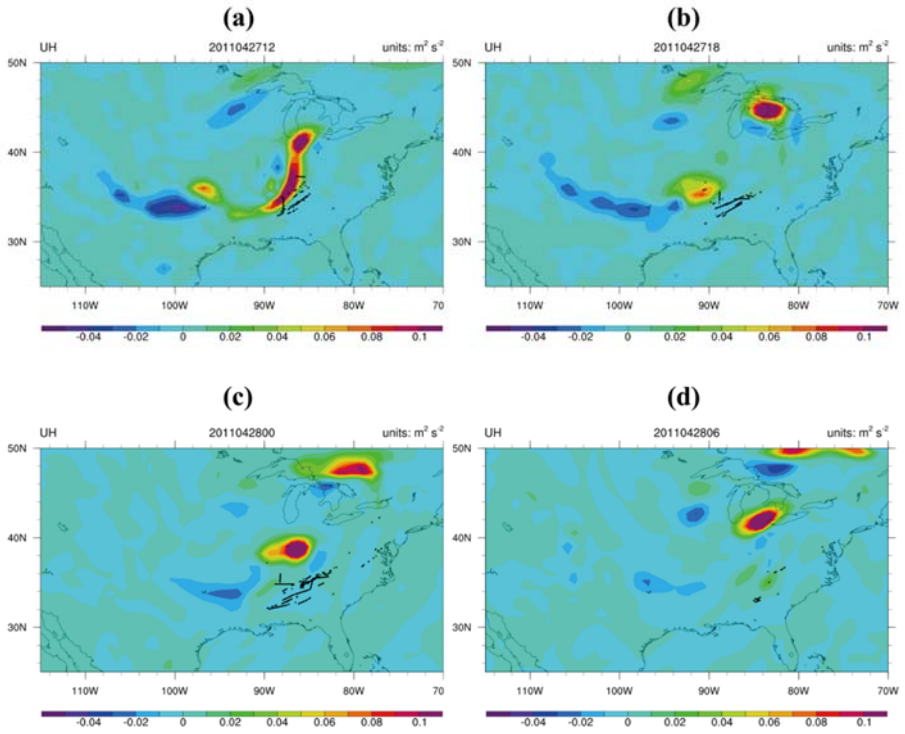

Figure 14. Horizontal distributions of UH (shading, 0.~~02~~ 01 $m^{-2}s^{-2}$ interval) integrated over 850–500 hPa at (a) 1200 UTC 27, (b) 1800 UTC 27, (c) 0000UTC 28, and (d) 0600 UTC 28 Apr 2011. Black stars and lines are locations and tracks of tornadoes centered within 6 hours.

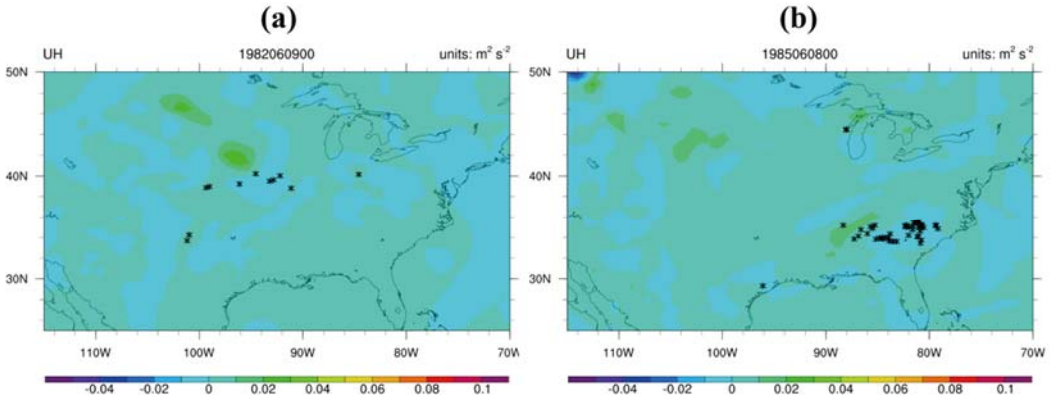

745

746 **Figure 15**. Horizontal distributions of UH (shading, 0.~~02~~ 01 $m^{-2}s^{-2}$ interval) integrated over 850–
747 500 hPa at (a) 0000 UTC 9 Jun 1982, (b) 0000 UTC 8 Jun 1985. Black ~~stars~~ asterisks are
748 locations of hail centered within 6 hours.

749

750

751

752

753

754

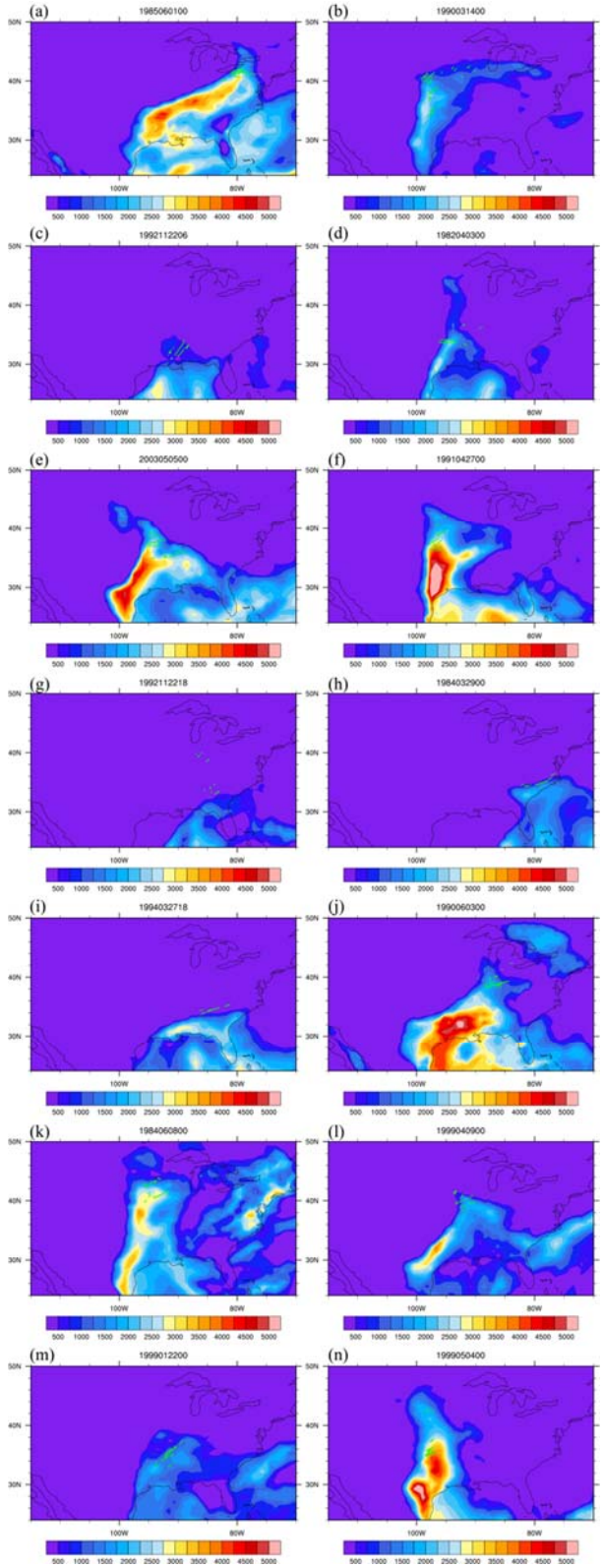

Figure 16. Same as Fig. 11 except CAPE (shading, 250 J/kg interval) for tornadoes.

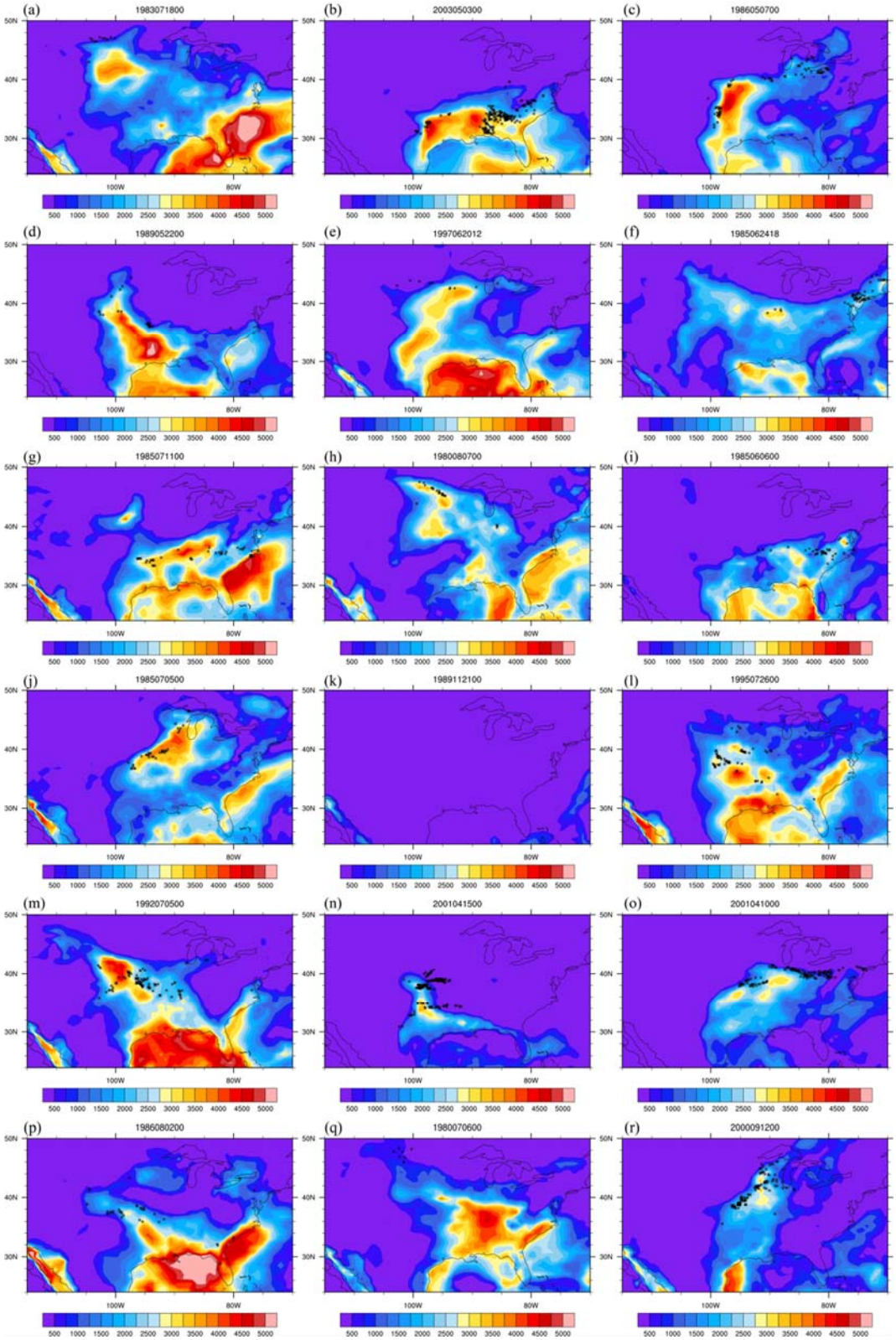

757

758 **Figure 17.** Same as Fig. 13 except CAPE (shading, 250 J/kg interval) for hails.

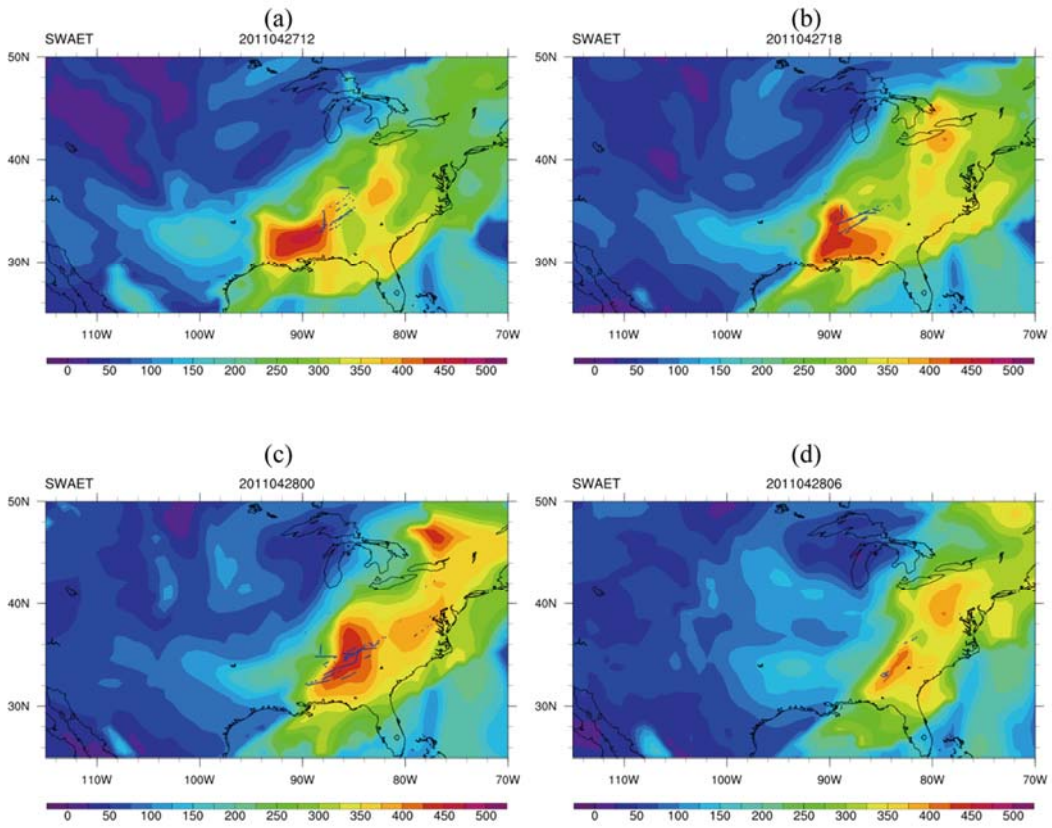

759

760 **Figure 18.** Same as Fig. 9 except SWEAT index at (a) 1200 UTC 27, (b) 1800 UTC 27, (c) 0000
761 UTC 28, and (d) 0600 UTC 28 Apr 2011.

762

763

764

765

766

767

768

769

770

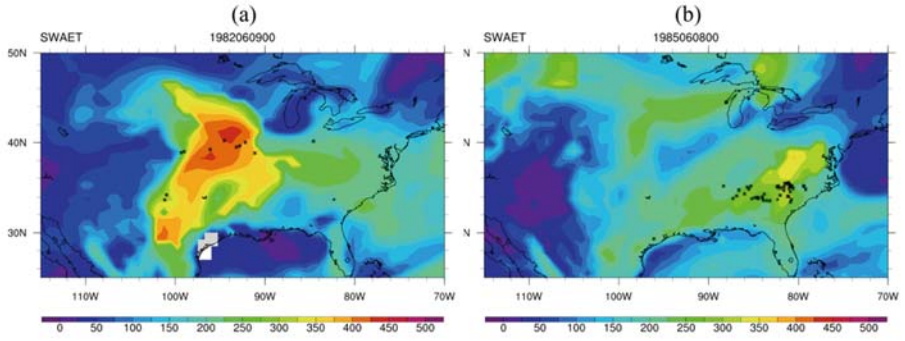

Figure 19. Same as Fig. 12 and Fig. 18 except SWEAT index at (a) 0000 UTC 9 Jun 1982 and (b) 0000 UTC 8 Jun 1985

790 **Table 1** A comparison of the ACI index central values (ºC) between tornadic and hail storms

	Tornadic outbreak cases				Hail day cases			
No.	Date	Positive	Negative	Difference	Date	Positive	Negative	Difference
1	3 Apr 1974				18 Jul 1983	4267.4	-4966.6	9234.0
2	1 Jun 1985	4273.3	-4249.9	8523.2	9 Jun 1982	4086.7	-9329.1	13415.8
3	14 May 1990	11063.6	-11938.5	23002.1	7 Jun 1985	4858.5	-2493.8	7352.3
4	14 May 1990				2 May 2003	4132.5	-5619.3	9751.9
5	22 Nov 1992	6831.7	-9987.9	16819.7	6 May 1986	7186.5	-3129.5	10316.0
6	3 Apr 1982	7261.9	-10562.1	17824.0	22 May 1989	5688.5	-3141.5	8830.0
7	5 May 2003	5648.1	-6707.9	12356.0	20 Jun 1997	3996.5	-5676.2	9672.7
8	27 Apr 1991	6790.7	-8004.2	14794.9	24 Jun 1985	2030.2	-7329.6	9359.8
9	22 Nov 1992	7170.3	-5503.3	12673.6	11 Jul 1985	2266.4	-9788.5	12054.9
10	27 May 1973				7 Aug 1980	5598.0	-7367.9	12965.9
11	29 May 1984	6502.5	-7682.3	14184.8	6 Jun 1985	2729.0	-4693.3	7422.3
12	27 May 1994	6721.4	-12159.0	18880.4	5 Jul 1985	5772.1	-4332.0	10104.1
13	3 Jun 1990	8358.6	-5855.4	14214.0	21 Nov 1989	2266.4	-8924.9	11191.3
14	8 Jun 1984	8615.8	-7827.8	16443.6	26 Jul 1995	4894.6	-2755.9	7650.5
15	9 Apr 1999	8840.3	-5920.4	14760.7	5 Jul 1992	3807.0	-7640.4	11447.4
16	17 Apr 1970				15 Apr 2001	5352.7	-9889.6	15242.3
17	21 Feb 1971				10 Apr 2001	8489.0	-1440.0	9929.0
18	22 Feb 1999	4168.5	-12656.4	16824.9	2 Aug 1986	3485.7	-7309.2	10794.9
19	20 Mar 1976				6 Jul 1980	3284.5	-5547.1	8831.6
20	3 May 1999	10722.8	-8937.3	19660.0	11 Sep 2000	7722.5	-5746.3	13468.8
	28 Apr 2011	10522.0	-6728.9	17250.9				
	Average	7355.0	-8428.0	15783.0	Average	4808.7	-5856.0	10451.7

791

792

793